A new CCD designed for curvature wavefront sensing

James W. Beletic[1], Reinhold J. Dorn[1], Thomas Craven-Bartle[1]
and Barry Burke[2]
[1]European Southern Observatory, [2]MIT Lincoln Laboratory

Abstract: We present a new CCD design that has been optimized for curvature wavefront sensing. Until now, only avalanche photodiodes (APDs) have been used as the detector in curvature wavefront sensing in astronomy, due to the strict requirements of very short integration time (250 μsec) and very low readout noise. The CCD we have designed and is being fabricated at MIT Lincoln Laboratory will achieve nearly the same AO system performance as APDs, at a fraction of the cost of APDs and without the long and uncertain single source procurement associated with APDs. In addition, this CCD will have higher quantum efficiency than APD modules and 1000 times the dynamic range of APDs, eliminating the need for neutral densities on bright objects. This article provides an introduction to curvature wavefront sensing, the curvature AO CCD design and results of a detailed computer simulation of the AO system performance.

Keywords: adaptive optics, CCDs, wavefront sensing

1. INTRODUCTION

The quality of images and spectra taken at ground-based astronomical observatories is degraded by distortions in the Earth's atmosphere. Rather than achieving diffraction-limited resolution, large ground-based telescopes at the best sites seldom achieve image quality better than the diffraction-limit of a 20 cm diameter telescope (0.5 arc sec in the visible, 0.5 μm wavelength). This blurring, which is due to temperature inhomogeneities in the atmosphere, is called atmospheric **seeing**. If the seeing could be eliminated, an 8-meter telescope would be able to achieve 0.013 arc sec resolution in the visible and 0.057 arc sec resolution in the K-band of the

infrared (2.2 μm). Compensation of the atmospheric seeing can be achieved using the technology of **adaptive optics** (AO), a technique which is being pursued by every major ground-based observatory. A good general reference is [1]. As it is more difficult to correct distortions at shorter wavelengths, in most cases astronomical observatories are only attempting to implement AO for infrared wavelengths. Figure 1 presents a simplified schematic of an adaptive optics system.

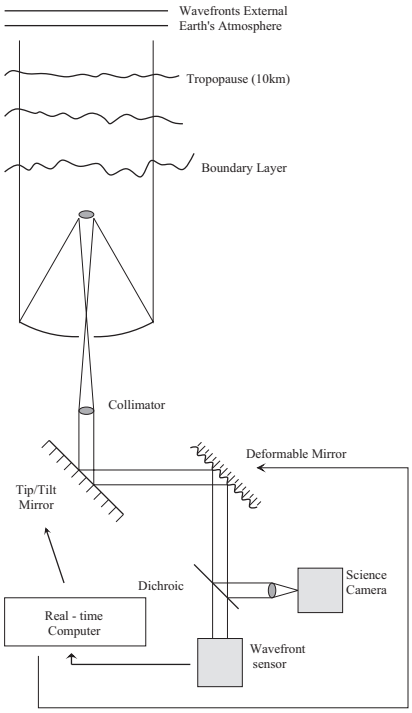

Figure 1. Schematic diagram of a "generic" adaptive optics system

The most precious signal in an AO system is the signal detected by the **wavefront sensor** (WFS). In many cases, the quality of the WFS signal determines the quality of the entire AO system operation. The WFS is located in the light path after the **deformable mirror** (DM), so that the WFS measures the residual wavefront distortion. The WFS signal is processed by the real-time computer and commands are sent to the DM so as to produce a flat wavefront at the WFS. Since the atmospheric distortion changes on timescales of 10 to 30 msec, the WFS must measure the wavefront distortion in a very short time; exposure times as short as 1 msec are desired. Due to the short exposure time, there is a limited number of photons available to the

WFS in each frame, especially for the distant and faint objects that are studied by large telescopes. *Thus, the primary limit to the performance of an adaptive optics system is the photon noise of the signal at the wavefront sensor*. Ideally, the only limit to the WFS performance is photon noise. Readout noise of the WFS should be minimized, and if possible, completely eliminated. Thus, the two most basic requirements for adaptive optics wavefront sensors are:

- high quantum efficiency,
- very low readout noise.

There are two other very important requirements for wavefront sensors:

- ability to take very short exposures,
- fast readout speed.

Ideally, the only phase lag in an AO system is the time needed for the WFS exposure. For photon counting detectors, such as avalanche photodiodes (APDs), there is effectively no delay due to readout time. Thus, when designing a CCD for wavefront sensing, it is very important to reduce the readout time so as to minimize phase delay errors.

There are several ways to measure the wavefront distortions, including Shack-Hartmann, shearing and Mach-Zender interferometry, pyramidic and curvature [2-5]. At this time, only two approaches are widely used for wavefront sensing in ground-based astronomical AO systems: Shack-Hartmann and curvature. Although curvature wavefront sensing is used in two of the most successful astronomical AO systems [6], the operation of a curvature WFS is not widely understood. To understand our new CCD design, one must first understand curvature wavefront sensing. Therefore, we include a section which gives a short overview of curvature WFS.

2. SHACK-HARTMANN AND CURVATURE WAVEFRONT SENSORS

Figure 2 presents a schematic of Shack-Hartmann and curvature wavefront sensing. Shack-Hartmann divides the wavefront into a two-dimensional array of square subapertures and places a lenslet in each subaperture to produce an array of images, one image from each subaperture. The location of the centroid of the image is a function of the tip and tilt of the wavefront in the subaperture. Usually, a CCD is used to detect the images of a Shack-Hartmann lenslet array. A minimum of 2 by 2 pixels, a quad cell, is needed to detect the image of each subaperture. To prevent

optical "crosstalk" between subapertures, a "guard ring" of at least one pixel is placed between subapertures. Thus, some Shack-Hartmann systems use 3 by 3 pixels per subaperture, as done at the Keck telescope. Another common arrangement is to have 4 by 4 pixels per subaperture (e.g. Starfire Optical Range). Some systems use 8 by 8 pixels in each subaperture [7]. Having more pixels gives more dynamic range to the WFS (i.e. greater tilts can be measured) and allows for more extended objects, but this is at the expense of the greater noise due to more pixels read out as well as longer readout time. To increase readout speed and lower the effect of readout noise, the 8 by 8 pixels can be binned into "superpixels" to mimic a smaller number of (larger) pixels [8].

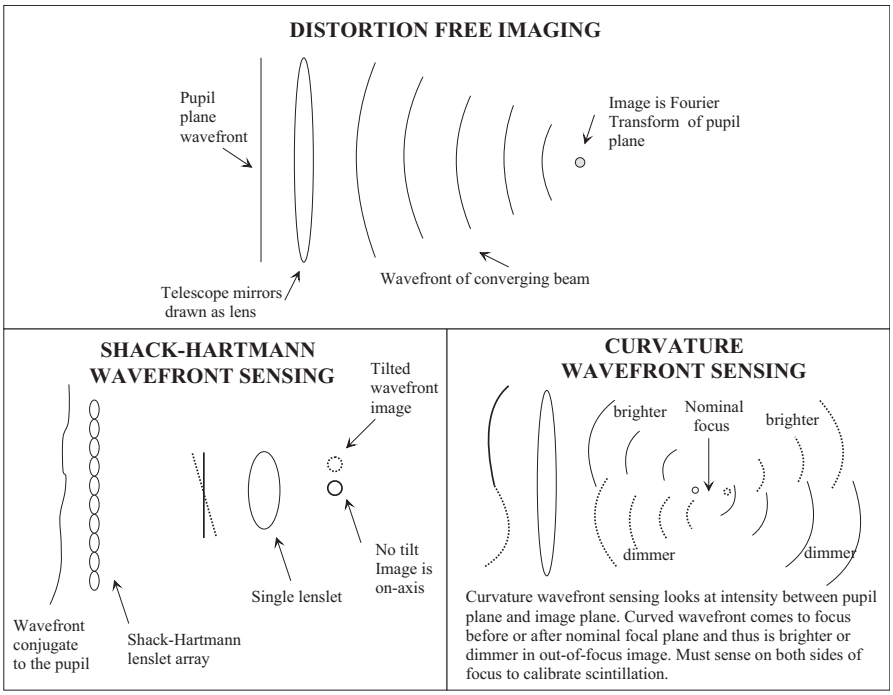

Figure 2. A schematic diagram of the principles of Shack-Hartmann and curvature wavefront sensing

Curvature wavefront sensing takes an entirely different approach. In curvature AO, the WFS measures an "image" at a location between the pupil plane and the image plane. If this image is before focus, it is called the **intrafocal image**; the image after focus is the **extrafocal image**, as shown in Fig. 3. The intrafocal image will be brighter in regions which have a positive curvature and the image will be darker in regions with negative

curvature. The intensity of the extrafocal image will be reversed relative to the intensity measured in the intrafocal image. In principal, only one out of focus image is needed to measure wavefront curvature. However, using both the intrafocal and extrafocal images makes a curvature system work better for several reasons: (a) there is automatic compensation of systematic errors - variation in quantum efficiency, electronic gain, etc., (b) there is compensation of atmospheric scintillation, and (c) the control algorithm is simple – move the deformable mirror so that the intensity difference is zero. In a curvature AO system, the goal is to make the intensities equal on both sides of focus – this will occur when the wavefront is flat.

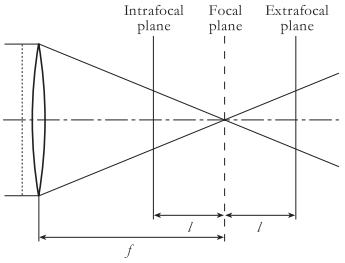

Figure 3. A flat wavefront focused by a lens, showing the intrafocal and extrafocal image planes on either side of the focal plane. Note that in actual implementation in curvature AO systems, the intra- and extrafocal planes are very close to the image plane, about 0.1% of the distance from the image plane to the pupil plane.

In order to derive the signal measured by the intrafocal and extrafocal images, we must look at the propagation of the electric field of the wavefront. Defining the direction of propagation from the pupil plane to the image plane as the direction z and the two orthogonal directions as x and y, the complex amplitude $U(x,y,z)$ of the field in a z-plane is the square root of the intensity $I(x,y,z)$ multiplied by the complex phasor of the wavefront phase $\phi(x,y,z)$:

$$U(x,y,z) = \sqrt{I(x,y,z)}e^{ik\phi(x,y,z)} \qquad (1)$$

where k is the wavenumber $(2\pi/\lambda)$ and λ is the wavelength of the light. The propagation of this field over short distances, i.e. in the near field, is defined by the **irradiance transport equation**:

$$\nabla I \cdot \nabla \phi + I\nabla^2 \phi + \frac{\partial I}{\partial z} = 0 \qquad (2)$$

where the gradient $\nabla = \frac{\partial}{\partial x} + \frac{\partial}{\partial y}$ and the Laplacian $\nabla^2 = \frac{\partial^2}{\partial x^2} + \frac{\partial^2}{\partial y^2}$. The last term in the Eq. (2), $\frac{\partial I}{\partial z}$, is the change in intensity as a function of propagation in the direction z. The change in intensity is the result of two terms:

- $\nabla^2\phi$ is the second derivative of the wavefront, i.e. the *wavefront curvature*
- $\nabla I \cdot \nabla\phi$ is the tilt of the wavefront – this term is only significant where the intensity is rapidly varying, which is at the edge of the pupil.

The change in intensity from intrafocal to extrafocal planes is due to the curvature of the wavefront over the pupil and the tilt of the wavefront at the pupil edge. The usefulness of this signal for adaptive optics was first recognized by Francois Roddier [9] and he first presented a system concept for wavefront sensing [10]. Using the vector $\vec{r}$ for the location *x,y* in a *z*-plane, I_1, I_2 for the intrafocal and extrafocal images, and *l* for the intra- and extrafocal distances, Roddier used the geometrical optics approximation to derive the curvature signal as,

$$S(\vec{r}) = \frac{I_2(\vec{r}) - I_1(-\vec{r})}{I_2(\vec{r}) + I_1(-\vec{r})} = \frac{\lambda f(f-l)}{2\pi l}\left[\nabla^2\phi\left(\frac{f\vec{r}}{l}\right) - \frac{\partial\phi}{\partial n}\left(\frac{f\vec{r}}{l}\right)\delta_c\right] \qquad (3)$$

where *f* is the telescope focal length, $\frac{\partial}{\partial n}$ is the derivative in the outward pointing radial direction and δ_c is a linear impulse function at the edge of the pupil (both at the outer edge of the primary and the inner edge due to secondary obscuration). Since tilt is only sensed at the pupil edge and the curvature signal is sensed over the entire pupil, this approach of sensing wavefront distortions is called **curvature wavefront sensing**.

An example of the way that a curvature wavefront sensor senses tilt is shown in Figure 4, a schematic drawing that shows the propagation of a flat, but tilted wavefront. The example is exaggerated since *l* is shown to be about 30% of the focal length, 250 to 500 times greater than an actual implementation.

A more realistic curvature signal is shown in Figure 5, which presents a Kolmogorov atmospheric wavefront distortion, intrafocal and extrafocal

images and the curvature signal. These signals were generated using a computer simulation.

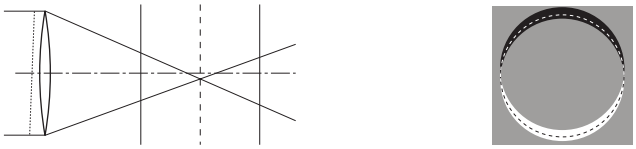

Figure 4. Propagation of a flat but tilted wavefront, shown left and the resulting curvature signal, shown right - grey is a curvature signal of zero, white is positive and black is negative. The dashed line in the right picture shows the outline of the pupil.

In Fig. 5, the AO loop is not running and thus the curvature signal extends well beyond the pupil. The speckle structure of the out of focus images is partially due to the single wavelength, and integration over the 400-1000 nm bandpass of a silicon sensor would have a smoother structure.

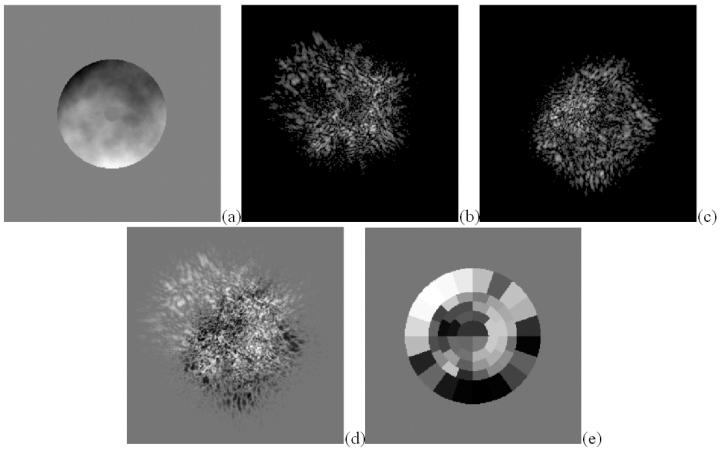

Figure 5. Computer simulation of curvature wavefront sensing: (a) wavefront distortion, (b) intrafocal image, (c) extrafocal image (d) curvature signal at high resolution, (e) curvature signal binned into 60 subapertures. Simulation parameters: 0.66 arc sec seeing (at 500 nm), sensing wavelength = 700 nm (monochromatic), out of focus distance = 25 cm, telescope focal length = 400 m, telescope diameter = 8 m with 14% obscuration from 1.12 m diameter secondary. Photon noise has not been simulated – all signals are "infinite" light level.

3. IMPLEMENTATION OF A CURVATURE WAVEFRONT SENSOR

One way to implement a curvature WFS would be to split the light into two halves and send one-half to a detector before focus and one-half to a detector after the focal plane. However, it would be better to have the same pixel sense the light from each subaperture on both sides of focus. This would remove all systematic errors such as pixel quantum efficiency and electronic gain from the curvature signal. However, if the same pixel is to be used on both sides of focus, it must sample both sides of focus "simultaneously", defined as "faster than the wavefront distortion or the scintillation changes". For correction in the infrared, sample times as short as 1 msec are required. For fainter objects, WFS frame rates as slow as 50 Hz may be useful, but it is important to remember that, even in these cases, the curvature WFS must be able to sample on both sides of focus at 1 kHz rate.

It would be impractical to attempt to physically move a detector the 50 cm between the intrafocal and extrafocal images at a 1 kHz rate. Instead most curvature AO systems in astronomy have adopted the approach pioneered by the U. Hawaii group [11,12], which is shown in Fig. 6. In this arrangement a membrane mirror oscillates in the image plane at 2 to 4 kHz rate, which makes the "detector plane" of the WFS detector alternately conjugate to the intrafocal and extrafocal images. *(In Fig. 6, the "detector plane" is the location of the lenslet array – the lenslet array is explained in section 4.)*

The relationship between the detector plane and the out of focus images is most easily explained via geometrical optics, using Fig. 7, which corresponds directly to Fig. 6; telescope mirror in Fig. 7 is same as the parabolic mirror after the deformable mirror in Fig. 6.

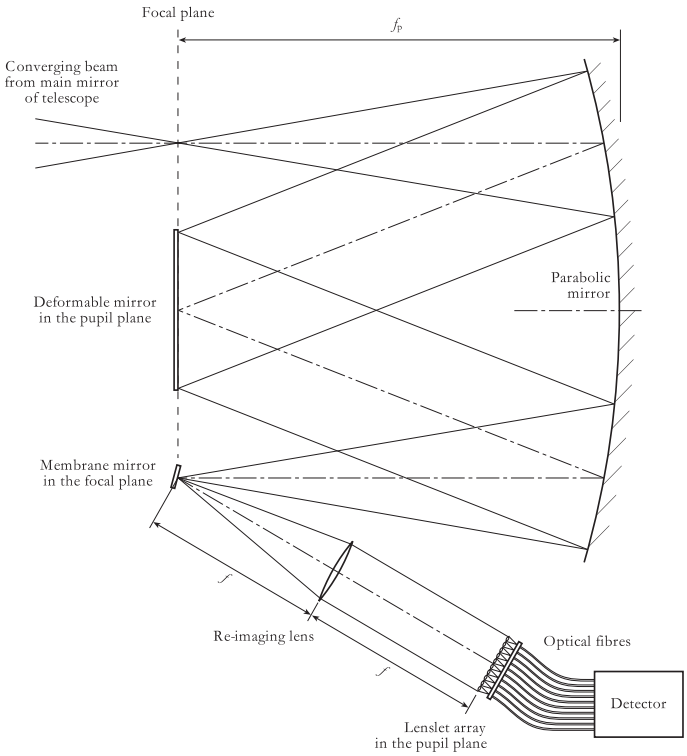

Figure 6. A schematic of the typical optical layout of a low light level astronomical AO curvature wavefront sensor

Fig 7 (a) shows the curvature WFS when the membrane is flat. Tracing the rays backwards from a point in the detector plane, we find that the detector plane is exactly conjugate to the pupil plane. With the membrane concave, and thus acting as a converging lens with focal length f_m, as shown in Fig 7 (b), the detector plane in conjugate to the intrafocal plane located a distance f_m before focus. Similarly, in Fig 7 (c), a convex membrane acts a diverging lens, making the detector plane conjugate to a distance f_m after the focal plane. Thus, the conjugate of the detector plane is defined by the focal length of the membrane.

The membrane is simply an acoustic speaker with reflective coating. It takes on a spherical shape with an amplitude of deformation that is a sinusoid as a function of time. It is important to compute how this sinusoid deformation converts to the membrane focal length.

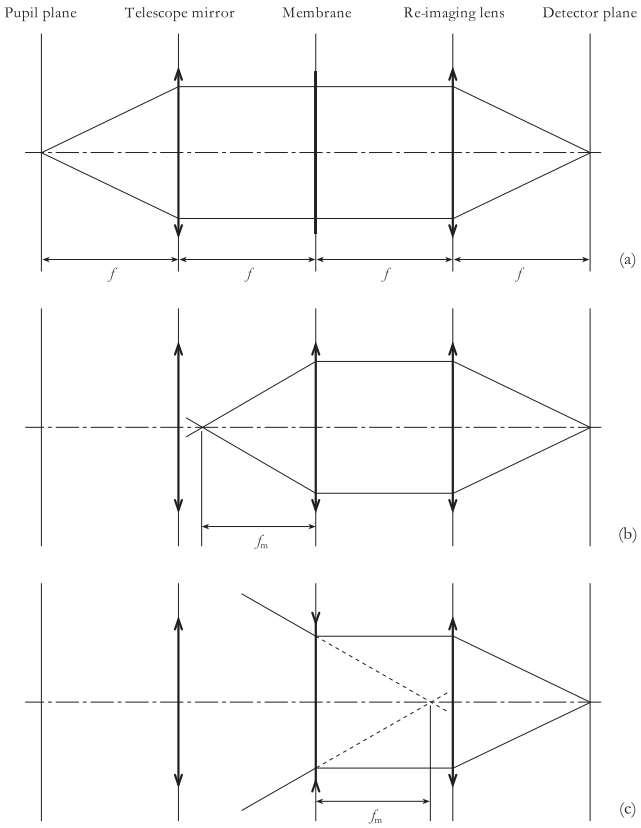

Figure 7. Geometrical optics analysis of the curvature wavefront sensor showing (a) case of flat membrane, (b) concave membrane and (c) convex membrane

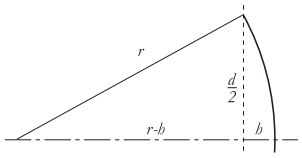

Figure 8. Geometry of the membrane mirror in a curvature AO system

Referring to Fig. 8, which shows the geometry of the membrane mirror, we see that

$$r^2 = (r-h)^2 + (\frac{d}{2})^2 \qquad (4)$$

where r is the radius of curvature of the membrane, d is the diameter of the membrane and h is the instantaneous amplitude of the membrane bow. Eq. (4) can be rewritten as,

$$r = \frac{h}{2} + \frac{d^2}{8h} \tag{5}$$

The focal length of the membrane is twice its radius of curvature, thus

$$f_{\mathrm{m}} = h + \frac{d^2}{4h} \tag{6}$$

Because h is typically much smaller than both d and f_m, the first term in Eq. (6) can be neglected. If the maximum amplitude of the membrane vibration is denoted A and the frequency at which it vibrates v, then $h(t) = A\sin(2\pi vt)$ and the focal length of the membrane as a function of time is,

$$f_{\mathrm{m}}(t) = \frac{d^2}{4A\sin(2v\pi t)} = \frac{f_{\min}}{\sin(2v\pi t)} \tag{7}$$

where $f_{min} = d^2/4A$, is the minimal focal length of the membrane.

Figure 9 plots the membrane amplitude and focal length as a function of time. The focal length function is radically different from a sinusoid. The detector plane literally "zooms" very quickly from the pupil plane, which is 400 meters from the image plane, to the minimal focal distance.

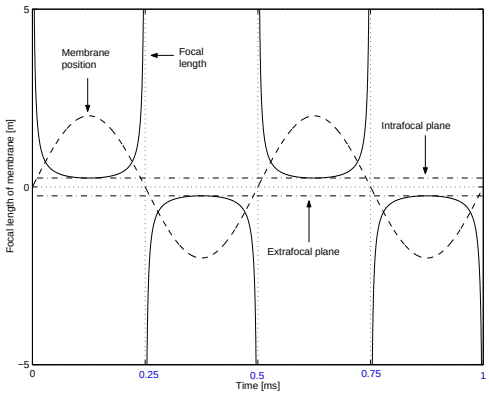

Figure 9. Membrane amplitude (dashed line) and membrane focal length (solid line) as a function of time for a 2 kHz membrane frequency with the minimum focal length set to 25 cm

Viewing out of focus images, one readily sees that there is not much difference between the pupil plane and the out of focus image for $f_m > 3$ meters. For a 2 kHz membrane oscillation and $f_{min} = 25$ cm, there is 13 μsec during each half cycle when $|f_m(t)| > 3$ meters. Thus, there is at least 10 μsec each half-cyle to allow a detector to switch between intrafocal and extrafocal integration states in the curvature WFS. This is an important parameter to remember when designing a CCD for curvature WFS.

Typical parameters for a membrane are: $d = 10$ mm, $f_{min} = 25$ cm, $A = 100$ μm. It is amazing what an oscillation of a small mirror by the width of a human hair can do!

The operation of a curvature WFS is easily explained in the language of Fourier optics. Referring to Fig. 6, at the membrane, the complex image field is multiplied by the membrane function. Since the membrane is purely reflective, the complex membrane function is unit amplitude with a centrally symmetric spherical phase term. At the detector plane, the field is given by the convolution of the pupil plane with the Fourier transform of the membrane function. If the membrane is flat, the membrane function at the detector plane is a delta function and the detector plane is exactly conjugate to the pupil plane. As the membrane increases its curvature, the Fourier transform of the membrane function grows in width so that the convolution integrates over a portion of the pupil. When the membrane curvature switches from concave to complex, the direction of the parabolic phase at the detector plane reverses. Thus, on one side of focus, positive wavefront curvature gives above average intensity at the detector plane and on the other side of focus, the intensity is weaker than average. The amplitude of the membrane oscillation is usually set so that the Fourier transform of the membrane has an effective width which is approximately the size of a single subaperture.

4. LOW LIGHT LEVEL OPERATION OF A CURVATURE WFS AND DETECTOR ISSUES

In this paper, we assume that the membrane will oscillate at a frequency of 2 kHz. Due to the relatively low resonance frequency of the bimorph mirrors used for curvature AO, the fastest update rate to a mirror will be 1 kHz. However, at the lowest light levels, there may be as few as 1 photon per subaperture for every 2 cycles of the oscillating membrane and the curvature WFS may need to operate as slow as 50 Hz frame rate. Thus, a

curvature WFS detector will need to integrate the light on each half-cycle for 2 to 40 cycles of the membrane. Each half cycle lasts 250 μsec and to minimize time delay, it is highly desirable to be able to read out the detector within 250 μsec.

An APD detector is a good match to these requirements if only a small number of pixels is desired. APD modules achieve 70% quantum efficiency, can detect up to a few million photons per sec, and the APD module outputs a digital pulse 100 nsec after photon detection. The dark current of an APD module can be specified to be less than 100 counts per sec, but a 250 dark count/sec device is sufficient for all but the very darkest nights.

In order to use the smallest number of APD modules, a lenslet array is used to concentrate the light from each subaperture onto an optical fiber, which guides the light to the APD modules, shown as the "detector" in Fig. 6. The geometry of the subapertures is defined by the lenslet array – the geometry that ESO is using for the 60 element curvature systems is shown in Fig. 10 [13].

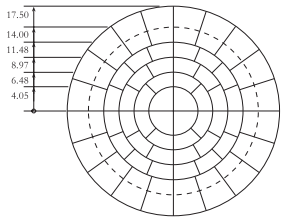

Figure 10. Subaperture geometry for ESO's 60 element curvature AO system. The numbers in the figure are the radii of the lenslet annuli in mm.

The subaperture geometry is defined to be annular in order to best match the circular telescope pupil. In specifying the exact layout of subapertures, the first choice is the number of annuli. Then, using computer simulations, various subaperture geometries are tested and the optimal arrangement is chosen. Generally, the chosen geometry is the one that equalizes subaperture areas. The outermost annulus has subapertures that extend beyond the pupil boundary, to capture light that is projected beyond the unaberrated pupil (c.f. Fig. 5). In ESO's design, there are 5 annuli and the lenslet array diameter is 25% larger than the pupil diameter. Refer to Fig. 5 to see an example of the curvature signal intensity integrated into the 60 subapertures.

Due to the 120 nsec dead time of the APD modules, 10% non-linearity is reached at 830,000 counts/sec, but this non-linearity can easily be compensated in the real-time computer. More important are the heating effects that occur at high count rates which can damage the APD module. Thus, the count rate should not exceed a few million counts/sec, which corresponds to an 8^{th}-9^{th} magnitude object in the ~1 m^2 subapertures of the 60 element AO system on ESO's 8-m telescope. For brighter objects, neutral density filters must be used with the APD modules.

There is only one commercial source for the highest quality APD modules - Perkin Elmer, formerly known as EG&G Canada. This firm has a history of long delivery time for APD modules. In the past, individual APD modules cost $3000 each, but recently several institutes have been quoted a price of $1800 for orders of large quantities (≥100) of the 250 dark count/sec modules. Thus, for a 60 element curvature AO system, the cost of APD modules is about $108,000.

Due to the large number of 60 element AO systems that ESO is implementing at the VLT telescopes (at least 7, when spare parts are counted), and concerns about APD cost and delivery schedule, ESO began investigating a specially designed CCD as the detector in its curvature WFS.

5. DESIGN CONSIDERATIONS FOR THE CURVATURE WFS CCD.

The requirements for the curvature WFS CCD are as follows:

1. 60 integration areas.
2. High quantum efficiency (peak greater 80%).
3. Very short exposure times (250 μsec) with "long" integration times (1 to 20 msec, 2 to 40 cycles of a 2 kHz membrane).
4. Ability to switch between half-cycle integrations within 10 μsec.
5. Ability to store half-cycle frames on-chip while integrating other half-cycle frames.
6. Lowest possible noise: 2 electrons maximum, < 1 electron desired (including all sources – dark current, readout noise, etc.).
7. Read out all pixels within 250 μsec.

The key to making a CCD work in this application is on-chip integration. In order to fulfill the requirements, we have utilized the following design options:

a. Use of superpixels, i.e. bin on-chip, to loosen alignment tolerances.
b. Lay out pixels on a grid to lower risk (keep it simple!), using fibers to feed from the lenslet array to the CCD, as is done with APD modules.
c. Use multiple readout ports to have slower readout rates and lower readout noise.

Note that a previous attempt was made to design a CCD for curvature wavefront sensing [14]. Frontside versions of the CCD were fabricated, but it has never been fully tested. However, to our knowledge, that version of a curvature WFS CCD will not be useful since it fails to fulfill several requirements: it can not integrate half-cycles on chip, it can not switch between half-cycles within 10 μsec, it does not have a 2 electron noise amplifier, and it can not read out in 250 μsec.

We believe that our newly designed CCD, named **CCID-35,** will fulfill all of the requirements.

This CCD has the ability to shift intrafocal and extrafocal photoelectrons integrated in a **superpixel** into charge storage areas on either side of the superpixel. The CCD can then be read out relatively slowly while the next integration starts on the chip.

The readout noise for the CCD is one of the most critical parameters for use in a curvature WFS. At low light levels, 14^{th} magnitude and fainter stars, 1 to 2 electrons noise at a readout speed of 50,000 pixels/port/sec is required. We have demonstrated this very low noise (1.9 electrons) at ESO with a MIT/LL CCID-20 at an even higher readout speed of 100,000 pixels/port/sec. The same output amplifier is used in the CCID-35.

In the following sections, we present the CCD design and implementation and the results of a detailed computer simulation to demonstrate the CCD should achieve nearly the same performance as the APD modules.

5.1 Architecture of the CCD

The CCD consists of 80 **unit cells** where the light from each subaperture will be focused. The transfer of light to the CCD can be done by a molded lenslet array directly or via fiber feed as done for APDs. For the first prototype we will use the fiber feed approach since it is difficult and costly to design a lenslet array which relays the radial geometry of the pupil image directly onto the grid structure of the CCD.

Figures 11 and 12 show the schematic layout of one of the **unit cells**. Figure 13 explains a **unit column**, consisting of ten unit cells and the associated readout amplifier. Figure 14 gives a schematic overview of the complete **device** consisting of eight unit columns, each with its own amplifier and the functional wiring of the device.

The CCID-35 also features a separate tip/tilt sensor integrated on the device. The results of our computer simulation (section 7) showed that a separate tip/tilt sensor would improve system performance for 60 element curvature AO. The best way to measure tip/tilt is with a quad cell detector in the image and therefore we required 4 superpixels on the tip/tilt sensor. The light from the quad cell can be relayed via fiber as for the curvature WFS detector.

5.1.1 Layout of one unit cell

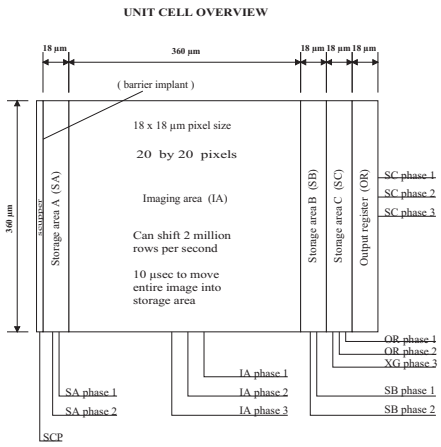

Figure 11. CCD design - unit cell overview

Figure 11 shows a functional drawing of a **unit cell**, with an integration area made of 20x20 pixels, each 18 μm square. These form an **imaging area** (IA) of 360 by 360 μm for each subaperture, large enough to focus the light without optical crosstalk to other pixels. These pixels will be binned by rows into the storage areas SA and SB. The storage areas are small compared to the imaging area, being only one pixel wide.

The SA and SB storage areas are used as a memory to store charge from the imaging area for multiple cycles of the membrane. After integration is completed the charge is moved into SC and then into the serial register for readout.

The complete imaging area can be shifted into a storage area within 10 μsec, during the relatively flat portion of the membrane oscillation, i.e. when $|f_m| > 3$ meters, as discussed in section 3.

A minimum number of clock phases is used to move and store the charges in the storage areas. Storage SA and SB have only 2 phases to store and move the charge. Three phases are needed for the storage area SC (SC1, SC2, XG), since a transfer gate is required as a barrier between SC and the serial register.

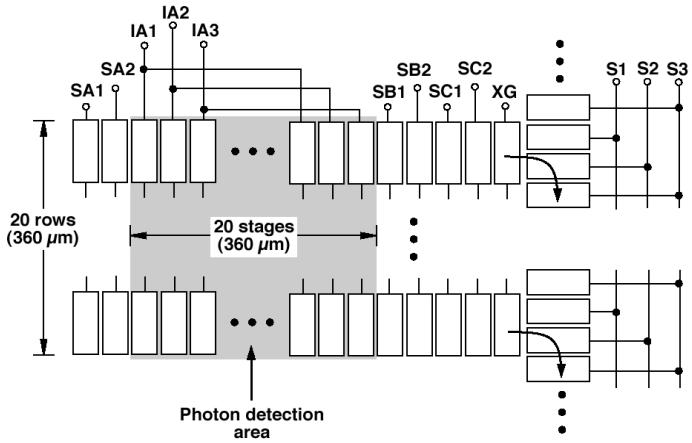

Figure 12. CCD design - superpixel architecture

5.1.2 Layout of one unit column with associated readout amplifier.

Figure 13 shows the layout of one **unit column** and the architecture of the associated readout amplifier. Ten unit cells in the vertical direction are combined to form one unit column.

There are only 3 prescan pixel in the serial register. Since each unit column is a collection of 10 unit cells and we only need to use 8 of the unit cells, we have the possibility to leave the first 2 cells empty to "warm up" the electronics for the 8 cells with light. If there is no need to warm up the electronics, we will put the spots close to the output amplifier and save the warmup time. In addition, the two extra cells will give us flexibility to avoid cells with traps.

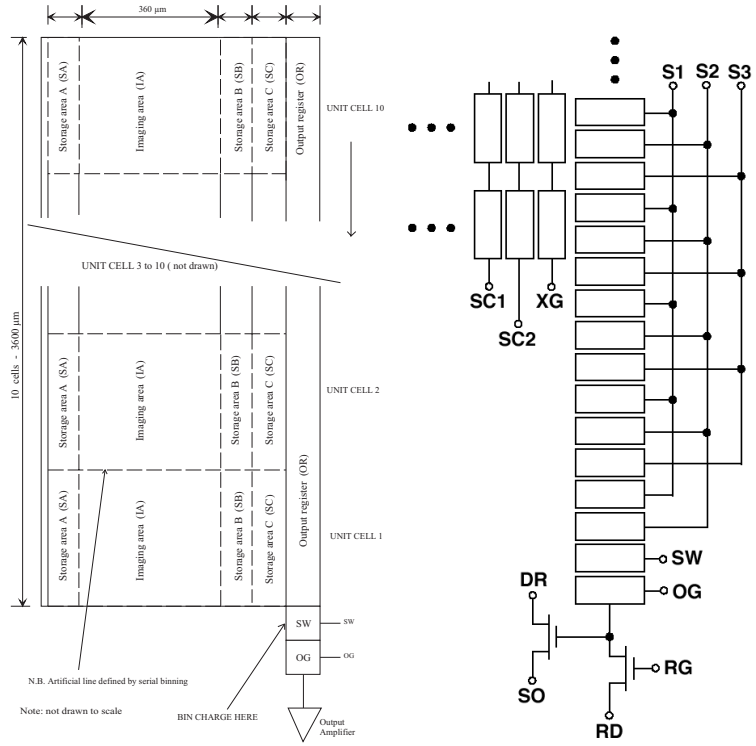

Figure 13. Unit column design - 10 combined unit cells and schematic diagram of the output amplifier circuit.

5.1.3 Tip/tilt sensor

Since simulations showed that for a 60-element curvature system Strehl is improved with separate tip/tilt sensing, the device features a tracker chip to be used as tip/tilt sensor. The tracker chip simply integrates charge and reads out; there is no need for storage area SA, SB and SC.

The tip/tilt sensor only has clocks IA1, IA2 and IA3 and XG. The tracker is a bit wider (24 pixels) since we expect to get at least 50 photoelectrons into each "cell" of the tracker chip; the extra rows provide tolerance for alignment and the use of larger fibers. Since we only need 4 subapertures in the tracker, it has a reduced length of 160 pixels.

The tip/tilt sensor is clocked completely independent of the curvature WFS CCD portion of the device. We can integrate and read out this tip/tilt array at a different rate, although for noise reasons we might synchronize the clocks of both arrays.

5.1.4 Layout of the curvature CCD, the CCID-35

To summarize the design, each superpixel consists of 20x20 pixels, where a pixel is 18 x 18 microns in size. The total height of each column is 10 superpixels or 200 pixels. There are 8 columns for a total of 80 superpixels and an independent tip/tilt sensor array. Figure 14 shows the CCD design of the curvature wavefront sensor array. The total width of each unit column, including the gap, is 550 μm. The tracker has the same width also.

There are substrate ground connections between the output circuit and the bottom of the imaging pixels to ensure good isolation of the clock waveforms from the output circuit. There is a **scupper** on the chip between each column to keep stray photocurrent and dark current from leaking into the pixels. Our experience with the CCID-20 [15] was that its 3 micron wide scupper does not fully capture all stray electrons. Therefore, we made the scupper on the CCID-35 10 microns wide. The output gates from the 8 outputs of the CWS-array are connected together on the chip to minimize the pin count and simplify packaging.

All of the corresponding clocks and bias lines for all unit columns are wired together on chip. Also the corresponding drive voltages for the

amplifiers circuits are wired together. Only the drain voltages for the output amplifier are brought out separately to be able to optimize noise and linearity for each amplifier individually.

Since we want to be able to move single electrons with good CTE, there is a notch in the channel. This is a standard feature of the CCID-20 and it reduces the ability of traps to capture electrons. This notch or trough is 2 microns wide in the image pixels and 3 microns wide in the serial pixels. The charge transfer inefficiency (CTI), for Fe-55 (1620 e-), was measured for a CCD of similar design to be $< 10^{-6}$ [16]. Measuring CTI for 2 electron charge packets is more problematic. However MIT/LL has measured CTI on proton-irradiated parts as a function of packet size down to 30 e- and found that the CTI varied approximately as the packet size to the -1/2 power. Assuming this variation is true for packets as small as 2 electrons, we would expect CTI $< 3 \times 10^{-5}$. For 200 transfers this implies 99.4% cumulative transfer efficiency.

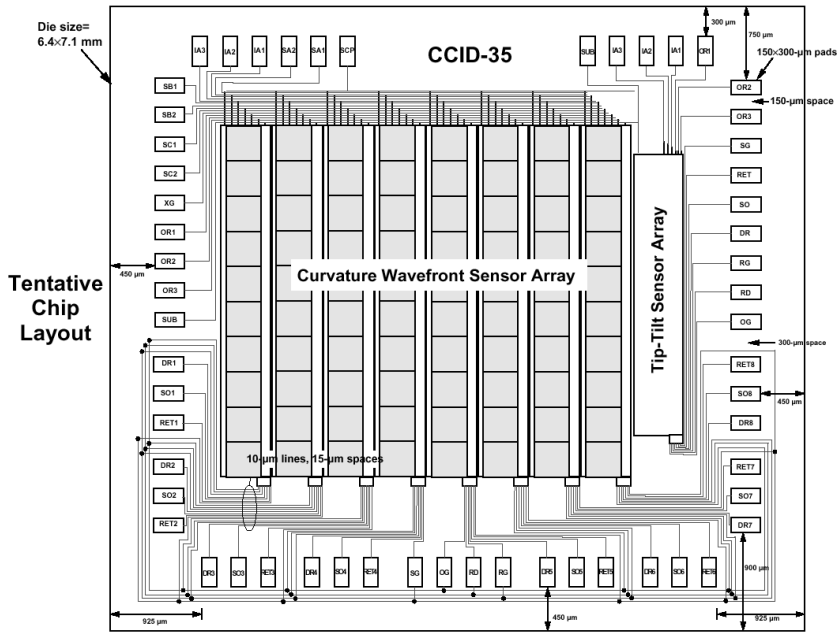

Figure 14. CCD design - curvature wavefront sensor array. The design consists of 80 unit cells. Ten unit cells are combined into a unit column. Each of these unit columns has an amplifier at the "bottom" end of the serial register. One the right side of the device is the tip/tilt sensor.

The **read noise** for the CCD should be as low as possible, preferably under 2 electrons at 50 kpixel per second. We will operate the CCD electronics at high gain (0.1 to 0.25 electrons / digital number). We decided to put the same amplifier on the CCD as for the MIT/LL CCID-20. This is a conventional floating diffusion amplifier or gated charge integrator. A JFET transistor, a U309, follows the output of the MOSFET. The U309 is located off chip and boosts the signal to the preamplifier. We expect a sensitivity of around 20 μV per electron. Figure 15 shows the amplifier design.

Parallel shift speed up to 3 MHz and serial shift speed up to 4 MHz is possible with this device, more than fast enough for a 2 kHz membrane frequency. With the high responsivity of the MIT/LL amplifier design, the amplifier full well is around 100,000 electrons. We expect good **linearity,** better than 1%, up to the full well.

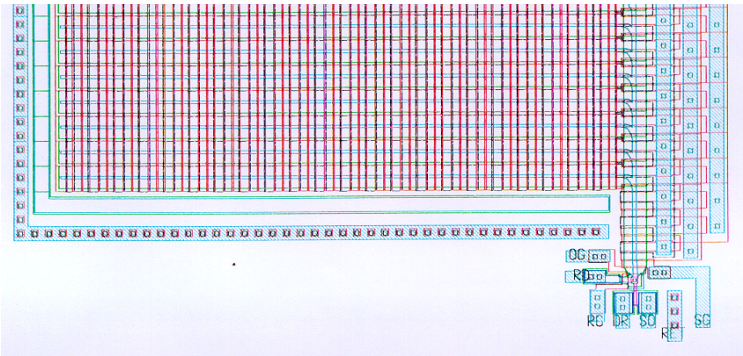

Figure 15. CCD design - CCID-35 amplifier design

The **cosmetic quality** is an important issue for this application. Since the CCD is small and many devices will be produced, we expect to be able to test and find devices that are cosmetically perfect.

For the thinned, back illuminated, CCD devices, there will be the same coating as for the MIT/LL CCID-20 (QE peak up to 90%). Figure 16 shows the **quantum efficiency** measurement of a CCID-20 [17]. We expect an equal or better QE for the CCID-35.

A very important requirement for the curvature AO CCD is the reduction of dark current to a negligible level. For the 360 x 360 micron superpixel we want to have less than 0.25 electron dark current per frame, so that readout

noise dominates. The slowest frame rate we will operate the device is 50 Hz, a frame time of 20 ms. Figure 16 shows the calculated dark current versus temperature using the following equation [18]:

$$N_d = 2.5 \cdot 10^{15} N_o d_{pix}^2 \, T^{1.5} \frac{-E_g}{e^{2kT}} \qquad (8)$$

were N_d is in electrons/pixel/s, N_0 is the dark current in nanoamps per square centimetres at room temperature (T_o), d_{pix} is the pixel size in centimeters, T is the operating temperature in Kelvin, E_G is the band gap energy in eV and k is the Boltzmann constant. For the CCID-35 we assumed N_0 to be 1 nA at a room temperature of 300 K. The band gap energy varies with temperature and is given by

$$E_g = \frac{7.021 \cdot 10^{-4} T^2}{1108 + T} \qquad (9)$$

In figure 16, the dashed line is dark current per superpixel per 20 ms, the solid line is dark current per pixel per second. The CCD must be cooled to a temperature of 192 Kelvin or -81°C to achieve a dark current of 0.25 electrons per superpixel at 50 Hz frame rate. Thus we will use liquid nitrogen to cool the CCD.

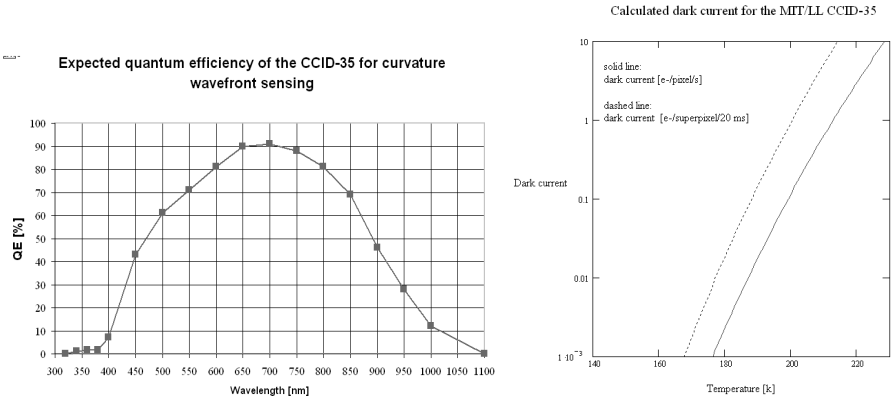

Figure 16. CCD design - expected quantum efficiency and calculated dark current for the CCID-35.

5.1.5 Expected CCD performance

Readout noise

The serial register of the CCD can be clocked at 3 MHz rate with no degradation of CTE. Thus, it will take about 70 μsec to move all 200 pixels of one unit column through the serial register. For a 250 μsec half-cycle of the 2 kHz membrane, there will be 180 μsec available for reading the 10 superpixels of a unit column, i.e. a pixel readout rate of 18 μsec per pixel.

At this rate, with high electronic gain (0.1 to 0.25 electrons per digital number), we expect to achieve ≤ 2 electrons noise.

Dynamic range

A good feature of the curvature CCD is its high dynamic range. For low light level situations, all photoelectrons of a subaperture will be binned into a single pixel. However, for bright objects, 20 pixels can be read out for each subaperture in each 250 μsec half-cycle.

Assuming that 10 pixels of each subaperture are filled to an average level of 75,000 electrons every half cycle, this is comparable to 3000 million photoelectrons per subaperture per second. The curvature WFS CCD has a dynamic range that is more than 1000 that of APD modules – while being linear to 1% over the entire range.

Field of view

Another good feature of the curvature CCD is its ability to sense a large field of view. The 100 μm core fiber being used in the initial testing is very conservative and is primarily being used to match the fiber used for APD modules.

However, it is important to note that a 200 μm core fiber would be feasible, which would result in a 6 arcsec field of view, double that accessible to an APD WFS system.

5.1.6 Driving the device and the CCD controller

We will use the FIERA CCD controller [19], developed by the Optical Detector Team at ESO to operate the device. FIERA is capable of reading

CCDs fast (up to 2 MHz per port) with noise limited by the CCD. FIERA has successfully demonstrated in the past to be able to run 16 ports in parallel at low noise [8].

Nevertheless any other CCD controller which is able to run at the desired readout speed will be suitable for operating the curvature WFS CCD.

6. FIBERFEED CONCEPT AND RELAY OPTICS

To transmit the light of each single subaperture of the lenslet array, a multi-mode fiber will be used. This fiber has a **numerical aperture (NA)** of 0.22, allowing us to input light with f-numbers of 2.27 or slower.

The fiber to be used will be a 100 micron core optical fiber with a numerical aperture of 0.22 +/- 0.02. This fiber works in the range of 450 nm to 1 μm with almost 100% efficiency at lengths up to 5 meters. These fibers have been fully characterised and tested by ESO. This 100 micron fiber is comparable to a 3 arcsec field of view in the VLT curvature AO system design.

An Offner Relay design consisting of two spherical, reflecting surfaces will be used to re-image the light of the fibers 1:1 onto the superpixels, as shown in figure 17. The support structure to attach the fibres to the input of the relay optics will be made of ceramic or invar. On this plate, the fibers will be glued into precision drilled holes.

Each individual fiber will be covered with a black sleeve and the fiber bundle put into a flexible tube. We decided to use relay optics for the prototype system to simplify the design testing. In parallel we are investigating mating the fiber directly to the CCD.

The designed optics has a maximum blur of 60 microns (100% encircled energy) over the entire field size of 3.6 x 4.8 mm, the light sensitive area of the CCD.

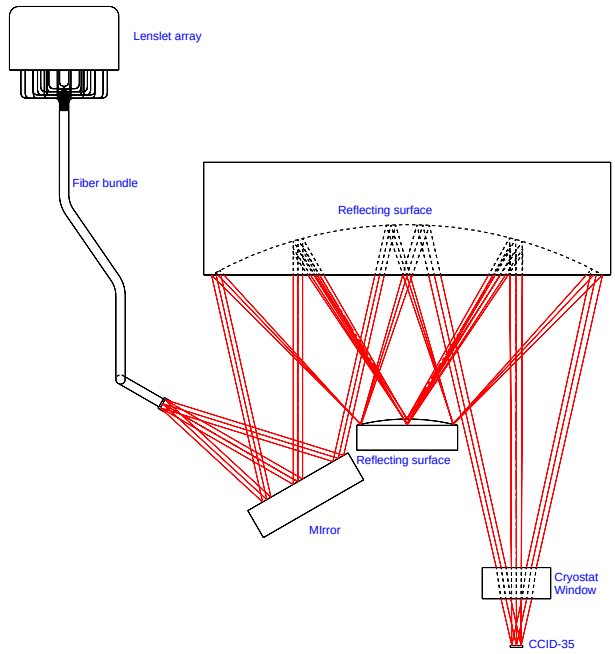

Figure 17. Relay optics to be used to reimage the light of the individual fibers onto the CCD.

7. COMPUTER SIMULATION OF CURVATURE WFS DETECTOR PERFORMANCE

We have developed a detailed computer simulation to compare the performance of the curvature WFS CCD with APD modules [20,21]. The simulation includes detailed models for atmospheric distortions (3 layers with different speeds, directions), telescope optics, bimorph deformable mirror and wavefront sensor optics.

The interaction matrix and control loop utilize the same algorithms as working curvature AO systems. The detector model includes random Poisson processes for modeling dark current and photon detection; readout noise is modeled as a zero mean Gaussian process. The simulation increments time in 15 μsec steps so that the effects of an evolving atmosphere and time delay of CCD readout are accurately modeled.

The quality of this simulation was verified by closely comparing its results with those of a simulation that has been validated with telescope data from the Hokupa'a and Pueo curvature AO systems.

The performance of the AO system is quantified by the Strehl ratio of the image in the K-band (2.2 μm) of the infrared as a function of the visible guide star magnitude. The Strehl is the ratio of the maximum intensity of the point spread function (PSF) relative to the maximum intensity of an aberration-free PSF.

The first result from the simulation was the discovery that, for a 60 element curvature AO system, the instantaneous Strehl was significantly higher than the integrated Strehl, as shown in Fig. 18 (left). The reduction of integrated Strehl is due to image wander, a problem that had been speculated for curvature systems with many subapertures [22].

The simulation was modified to include a separate tip/tilt sensor that used 20% of the light, which gave a significant improvement to integrated Strehl, as shown in Fig. 18 (right). This prompted us to include a tip/tilt sensor in the curvature AO CCD design (see section 5). Although there appears to be a clear advantage for using a separate tip/tilt sensor, there may be complications in co-aligning the curvature and tip/tilt sensors.

Thus, we have simulated the APD and CCD performance for systems with and without a separate tip/tilt sensor. The results are presented in Fig. 19, with Table 1 listing the parameters used for these simulation runs.

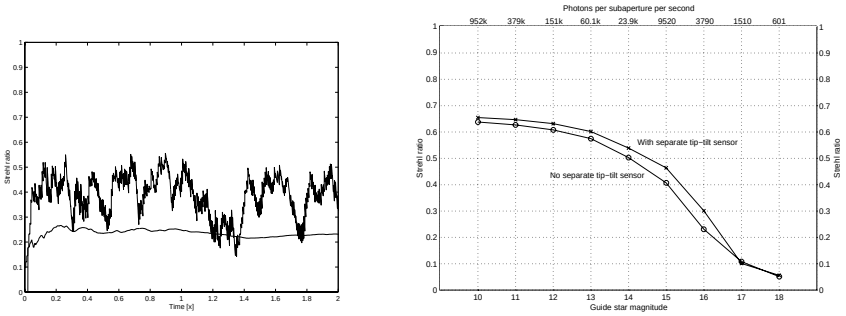

Figure 18. Left: Instantaneous and integrated Strehl ratios at 2.2 microns when using APDs and 16th magnitude guide star with no separate tip/tilt sensor. *Right:* Integrated Strehl as a function of guide star magnitude for APD detectors with and without separate tip/tilt sensor (which uses 20% of the light). The sky background is 19th magnitude per square arc sec and the APD dark current is 250 counts/sec.

For these simulation runs, the APD parameters are: 250 dark counts/sec, 70% quantum efficiency (including fiber losses), zero read noise. The CCD parameters are: zero dark counts/sec, 80% quantum efficiency (including fiber losses), 2 electrons read noise, 250 μsec delay. The sky background is 19th magnitude per square arc sec. A darker sky (21st mag / square arc sec) gives the same results but with slightly better Strehl achieved at guide star magnitudes 16 and 17.

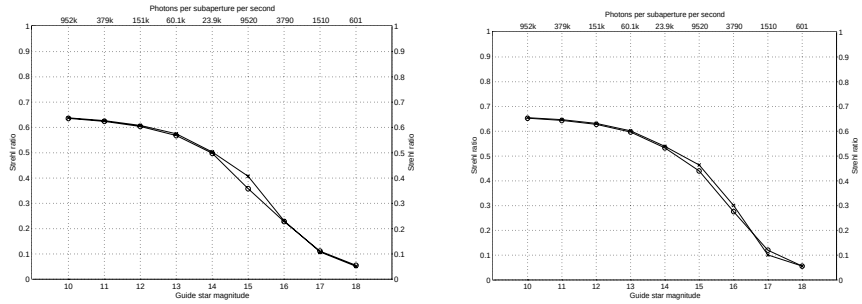

Figure 19. The left figure shows the performance of the APD and CCD without a tip/tilt sensor. On the right: Performance of the APD and CCD with a tip/tilt sensor that utilizes 20% of the photons.

The results from the computer simulation show that the curvature CCD should achieve the same performance as an APD, except at magnitudes 15 and 16, when the integrated Strehl is 2-5% higher for the APD-based system.

Guide star magnitude	Photon flux* per subaperture [1/s]	Integration time [ms]	Loop gain	Photon flux* per integration [1/s]
10	$952 \cdot 10^3$	2.0	0.60	1904
11	$379 \cdot 10^3$	2.0	0.50	758
12	$151 \cdot 10^3$	2.0	0.40	302
13	$60.1 \cdot 10^3$	2.0	0.30	120
14	$23.9 \cdot 10^3$	5.0	0.60	120
15	9520	5.0	0.50	47.6
16	3790	6.5	0.30	24.6
17	1510	15.0	0.30	22.7
18	601	40.0	0.30	24.0

* on the detector – to get number of photoelectrons, multiply by the detector QE.

Table 1. Parameters used in the Simulation

8. CONCLUSION

The CCD performance will be verified during 2000 with a frontside illuminated device and at the end of 2000, the first thinned devices should become available. After the non-redundant engineering phase of the CCD is completed, the relative advantages and disadvantages of the two detectors are anticipated to be as follows:

Advantages of a CCD-based curvature WFS (vis-a-vis APD modules):

- Cost (about half of an APD-based system, depending on number of subapertures)
- Procurement / delivery schedule (avoid single source APD supplier)
- Higher dynamic range (factor of 1000)

Disadvantages of a CCD-based curvature WFS (vis-a-vis APD modules):

- Liquid nitrogen dewar required to reduce dark current to a negligible level (but not a problem if LN2 needed for an IR imager)
- Slightly lower performance at guide star magnitudes 15 and 16

We believe that we have designed a CCD that can be used for curvature wavefront sensing in astronomical AO systems and that this CCD will achieve nearly the same AO system performance as an APD-based WFS.

9. REFERENCES

[1] Roddier, F.J. (1999). ed. (with 11 contributors). *Adaptive Optics in Astronomy*. Cambridge University Press, Cambridge (UK).

[2] Rousset, G. (1999). Wavefront sensors, In: *Adaptive Optics in Astronomy*, F.J. Roddier, ed. Cambridge University Press, Cambridge (UK), pp. 91-130.

[3] Tyson, R.K. (1991). *Principles of adaptive optics*. Academic Press, San Diego.

[4] Ragazzoni, R. (1996). Pupil plane wavefront sensing with an oscillating prism. *Journal of Modern Optics*, vol. 43, p. 289.

[5] Ragazzoni, R. and J. Farinato (1999). Sensitivity of a pyramidic wavefront sensor in closed loop adaptive optics. *Astronomy & Astrophysics*, vol. 350, p. 23.

[6] Roddier, F.J. and F. Rigaut (1999). The UH-CFHT systems. In: *Adaptive Optics in Astronomy*, F.J. Roddier, ed. Cambridge University Press, Cambridge (UK), pp. 205-34.

[7] Rousset, G. (2000). Status of the VLT Nasmyth Adaptive Optics System (NAOS). In: *Adaptive Optical Systems Technology*, Munich, Germany, March 27-31, 2000, Proceedings of SPIE, vol. 4007.

[8] Feautrier, P. and R. J. Dorn (2000). NAOS visible wavefront sensor. In: *Adaptive Optical Systems Technology*, Munich, Germany, March 27-31, 2000, Proceedings of SPIE, vol. 4007.

[9] Roddier, F.J. (1987). Curvature sensing: a diffraction theory, NOAO R&D Note No. 87-3.

[10] Roddier, F.J. (1988). Curvature sensing and compensation: a new concept in adaptive optics. *Applied Optics* ***27***, 1223-5.

[11] Graves, J.E. and D. McKenna (1991). University of Hawaii adaptive optics system III: wavefront curvature sensor. In: *Active and Adaptive Optics*, San Diego (California), July 22-24, 1991. Ed. M.A. Ealey, Proc. SPIE 1542, pp. 262-72.

[12] Graves, J.E., F.J. Roddier, M.J. Northcott and J. Anuskiewicz (1994). University of Hawaii adaptive optics system IV: a photon-counting curvature wavefront sensor. In: *Adaptive Optics in Astronomy*, Kona, March 17-18, 1994, eds. M.A. Ealey and F. Merkle, Proc. SPIE 220-1, pp. 502-7.

[13] Donaldson, R., D. Bonaccini, J. Brynnel, B. Buzzoni, L. Close, B. Delabre, C. Dupuy, J. Farinato, E. Fedrigo, N. Hubin, E. Marchetti, S. Stroebele, S Tordo (2000). MACAO and its application for the VLT interferometer. In: *Adaptive Optical Systems Technology,* Munich, Germany, March 27-31, 2000, Proceedings of SPIE, vol. 4007.

[14] Geary, J.C. and G.A. Luppino (1994). New circular radial-scan frame-storage CCDs for low-order adaptive optics wavefront curvature sensing. *Adaptive Optics in Astronomy*. Proc. SPIE 2201, pp. 588-595.

[15] Cavadore C. and R.J. Dorn (2000). Charge coupled devices at the European Southern Observatory - performance and results, these proceedings.

[16] Burke, B. (1999). MIT Lincoln Laboratory. Private communication

[17] Dorn R.J., J.W. Beletic, C. Cavadore and J.L. Lizon (2000). The optical detector systems for the blue and red arms of UVES, the echelle spectrograph for the UT2 Kueyen Telescope at the ESO Paranal Observatory, In: *Optical and IR Telescope Instrumentation and Detectors*, Munich, Germany, March 27-31, 2000, Proceedings of SPIE, vol. 4008.

[18] Janesick, J.R. (1997). CCD camera Design and Applications, Lecture Notes, University of California, Short course program.

[19] Beletic J., R Gerdes and R.C. DuVarney (1998). FIERA: ESO's new generation CCD controller, In: *Optical Detector for Astronomy*, James W. Beletic and Paola Amico ed., Kluwer Academic Publishers.

[20] Craven-Bartle, T.V. (2000). Modelling curvature wavefront sensors in adaptive optics. Master's thesis, Dept. of Applied Physics, Linköpings Universitet (Sweden).

[21] Craven-Bartle, T.V., R.J Dorn and J.W. Beletic (2000). Computer simulation of CCDs and APDs for curvature wavefront sensing. In: *Adaptive Optical Systems Technology*, Proceedings of SPIE, vol. 4007.

[22] Northcott, M.J. (1999). University of Hawaii, Institute of Astronomy, Private communication.